Quantification of fossil fuel CO_2 from combined CO, $\delta^{13}CO_2$ and $\Delta^{14}CO_2$ observations

Jinsol Kim[1], John B. Miller[2], Charles E. Miller[3], Scott J. Lehman[4], Sylvia E. Michel[4], Vineet Yadav[3], Nick E. Rollins[1], and William M. Berelson[1]

[1]Department of Earth Sciences, University of Southern California, Los Angeles, CA 90089, USA
[2]Oceanic and Atmospheric Administration Global Monitoring Laboratory, Boulder, CO 80305, USA
[3]Jet Propulsion Laboratory, California Institute of Technology, Pasadena, CA 91109, USA
[4]Institute of Arctic and Alpine Research, University of Colorado, Boulder, CO 80309, USA

Correspondence to: Jinsol Kim (jinsolki@usc.edu)

Abstract. We present a new method for partitioning observed CO_2 enhancements (CO_2xs) into fossil and biospheric fractions (C_{ff} and C_{bio}) based on measurements of CO and $\delta^{13}CO_2$, complemented by flask-based $\Delta^{14}CO_2$ measurements. This method additionally partitions the fossil fraction into natural gas and petroleum fractions (when coal combustion is insignificant). Although here we apply the method only to discrete flask air measurements, the advantage of this method (CO and $\delta^{13}CO_2$-based method) is that CO_2xs partitioning can be applied at high frequency when continuous measurements of CO and $\delta^{13}CO_2$ are available. High frequency partitioning of CO_2xs into C_{ff} and C_{bio} has already been demonstrated using continuous measurements of CO (CO-based method) and $\Delta^{14}CO_2$ measurements from flask air samples. We find that the uncertainty in C_{ff} estimated from the CO and $\delta^{13}CO_2$-based method averages 3.2 ppm (23 % of the mean C_{ff} of 14.2 ppm estimated directly from $\Delta^{14}CO_2$) which is significantly less than the CO-based method which has an average uncertainty of 4.8 ppm (34 % of the mean C_{ff}). Using measurements of CO, $\delta^{13}CO_2$ and $\Delta^{14}CO_2$ from flask air samples at three sites in the greater Los Angeles region, we find large contributions of biogenic sources that vary by season. On a monthly average, the biogenic signal accounts for -14 to +25 % of CO_2xs with larger and positive contributions in winter and smaller and negative contributions in summer due to net respiration and net photosynthesis, respectively. Partitioning C_{ff} into petroleum and natural gas combustion fractions reveals that the largest contribution of natural gas combustion generally occurs in summer, which is likely related to increased electricity generation in LA power plants for air-conditioning.

1 Introduction

The world's cities account for up to 70 % of global greenhouse gas (GHG) emissions, while covering less than 2 % of the Earth's surface (IPCC, 2014). Cities around the world have started implementing mitigation strategies to reduce carbon dioxide (CO_2) emissions and collaborate with each other in organizations such as the C40 Cities Climate Leadership Group (https://www.c40.org/) and the Global Covenant of Mayors for Climate and Energy (https://www.globalcovenantofmayors.org/). To support urban efforts, monitoring systems are necessary to evaluate and verify reductions attributable to specific mitigation strategies (Turnbull et al. 2022).

Current understanding of anthropogenic CO_2 emissions mainly derives from methods that estimate aggregate emissions in a domain using economic statistics such as total fuel sales or activity data such as total distance traveled for on-road vehicle emissions. These "bottom-up" methods provide specific location and process information that rely on mapping the source-specific emission factors and measurements of activities (e.g., McDonald et al. 2014; Gurney et al. 2019; Gately and Hutyra 2017; Super et al. 2020). In contrast, more recently "top-down" methods that quantify emissions from measurements of atmospheric CO_2 have been used to estimate emissions. These top-down approaches typically use either a mass balance technique where an initial estimate is not required (e.g. Mays et al. 2009; Cambaliza et al. 2014; Heimburger et al. 2017; Ahn et al. 2020) or an inverse/data assimilation approach where observations and a prior map of emissions are combined to generate a best estimate (e.g. Bréon et al. 2015; Staufer et al. 2016; Sargents et al. 2018; Turner et al. 2020; Lauvaux et al. 2016, 2020).

To estimate anthropogenic CO_2 emissions using top-down method, it is crucial to separate the fossil fuel signals from the biogenic signals, which can vary from negative (uptake) to positive (emission) across the annual cycle. Recent analyses of urban CO_2 suggest that biogenic emissions and uptake have significant magnitudes relative to fossil fuel fluxes, especially during the growing season (Sargent et al., 2018; Vogel et al., 2019; Miller et al., 2020). Previous top-down studies used biosphere models to estimate biogenic fluxes and then focused on determining the balance of emissions attributable to fossil fuel combustion assuming that the biogenic emissions are known (Sargent et al. 2018; Turner et al. 2020; Lauvaux et al. 2020). However, even with recent improvements in biosphere models (Wu et al. 2021; Gourdji et al. 2022) the actual magnitude and variability of these fluxes are still not well constrained (Hardiman et al., 2017; Winbourne et al.,

2022), potentially leading to unknown observational bias in the associated estimates of fossil fuel derived emissions.

Radiocarbon ($^{14}CO_2$) provides the ability to separate biogenic and anthropogenic CO_2 fluxes and mole fractions from an observational point of view (e.g. Levin, 2003; Turnbull 2006). Observational methods rely on the fact that fossil fuels and the resultant CO_2 produced during combustion are completely devoid of ^{14}C (i.e., $\Delta^{14}C_{ff}$ = -1000‰ on the widely used Delta scale; Stuiver and Polach, 1977). Measurements of $\Delta^{14}CO_2$, acquired at time scales of weeks to months, allow quantification of seasonal variations in biogenic and fossil contributions to the atmospheric CO_2 mole fraction (e.g., Djuricin et al. 2010; Miller et al. 2012; Turnbull et al. 2015). ^{14}C methods typically require air sample collection, preparation and analysis via accelerator mass spectrometry which limits the number of measurements, although a number of promising optical methods for in situ $^{14}CO_2$ measurement at natural abundance are currently being developed (Fleisher et al. 2017; Genoud et al. 2019; McCartt and Jiang 2022).

On the other hand, carbon monoxide (CO) is a widely used tracer that can be measured continuously in situ using high-precision optical analyzers (e.g. Vogel et al. 2010; Newman et al. 2013; Turnbull et al. 2015; Lauvaux et al. 2020). CO is often co-emitted with fossil fuel CO_2 (CO_2ff) during incomplete combustion. If the COxs:CO_2ff ratio (R_{ff}, where COxs is the CO enhancement above background) is well constrained, continuous CO measurements combined with R_{ff} can provide an estimate of continuous CO_2ff. A few studies have applied this method to estimate fossil fuel emissions for a moment in time during an airborne measurement campaign (Graven et al. 2009; Turnbull et al. 2011). However, this approach is challenging to identify interannual trends because R_{ff} at a site may vary significantly on timescales ranging from hours to years (Levin and Karstens, 2007; Vogel et al., 2010). CO:CO_2 emission ratio can vary by sources depending on the carbon content of the fuel and combustion conditions. Due to the impacts of atmospheric transport at a given observation site and the variability in the source combination in time and space, R_{ff} also varies in time and space. Additionally, CO produced from oxidation of volatile organic compounds (VOCs) can have an effect (Vimont et al., 2019).

Vardag et al. (2015) proposed dividing fossil fuel emissions further into two groups that may display less variability in CO:CO_2 emission ratio. If one group is well constrained by CO and the other by $^{13}CO_2$, each group can be identified by combining CO and $^{13}CO_2$ observations. Vardag et al. focused on separating traffic from non-traffic emissions, or biofuel emissions from the other

fossil fuel emissions. However, no significant benefit of combining CO and $^{13}CO_2$ was found because traffic and biofuel CO_2 do not produce distinct CO:CO_2 emission ratio or $^{13}CO_2$ isotopic signatures compared to the other CO_2ff source terms.

Here, we differentiate CO_2 signals from biogenic, petroleum and natural gas sources by combining CO, $\delta^{13}CO_2$, and $\Delta^{14}CO_2$ measurements. The combination of $\Delta^{14}CO_2$ and $\delta^{13}CO_2$ has been used previously to distinguish biogenic, petroleum and natural gas signals for air sampling events (Lopez et al. 2013; Djuricin et al. 2010) and at seasonal scale (Newman et al., 2016). In contrast, the combination of CO and $\delta^{13}CO_2$, which can both be measured at high frequency, enables source partitioning at higher temporal resolution. We demonstrate the agreement between the existing $\Delta^{14}CO_2$, $\delta^{13}CO_2$ and newly proposed CO, $\delta^{13}CO_2$ methods. This establishes the utility of the CO and $\delta^{13}CO_2$ in partitioning CO_2xs into fossil fuel and biogenic components, with further partitioning of fossil fuel sources into petroleum and natural gas sources, in the Los Angeles megacity.

2 Methods

Here, we describe two methods for separating fossil fuel and biogenic components from atmospheric CO_2 measurements in the complex urban environment of the Los Angeles megacity (LA). Section 2.2 describes our application of the method already described by Newman et al. (2016) using $\Delta^{14}CO_2$ and $\delta^{13}CO_2$ observations. The details of the new method utilizing CO and $\delta^{13}CO_2$ measurements are described in section 2.3. Briefly, we take advantage of the fact that the combination of the CO:CO_2 emission ratio and the $^{13}CO_2$ isotopic signature reveal a very distinct pattern for biogenic, petroleum and natural gas sources. However, this approach requires knowledge of the CO:CO_2 emission ratio and the isotopic signature of each source. We apply isotopic signatures reported by previous studies, and CO:CO_2 emission ratios are determined for LA using measurements of CO, $\delta^{13}CO_2$ and $\Delta^{14}CO_2$ from flask samples. Flask measurements are described in section 2.1 and the source apportionment from $\Delta^{14}CO_2$ and $\delta^{13}CO_2$ observations, which is used to derive CO:CO_2 emission ratios for each source, is described in section 2.2.

2.1 Measurements

We use measurements from air samples collected at 2 p.m. local standard time at three existing Los Angeles Megacity Carbon Project sites: University of Southern California (USC), California State University, Fullerton (FUL), and Granada Hills (GRA) (Miller et al., 2020). Air samples were collected from November 2014 to March 2016 using National Oceanic and Atmospheric Administration (NOAA) programmable flask packages (PFPs) and programmable compressor packages (Sweeney et al., 2015). The samples were sent back to the NOAA Global Monitoring Laboratory where greenhouse gases including CO_2 as well as CO mole fractions were measured using NOAA's high-precision/high-accuracy greenhouse gas measurement system (Sweeney et al., 2015). After the measurement, residual air is extracted from PFP flasks and CO_2 is isolated for ^{14}C measurement using established cryogenic and mass spectrometric techniques (Lehman et al., 2013). Samples are purified, graphitized and packed into individual targets at the University of Colorado, Boulder, Institute of Arctic and Alpine Research (INSTAAR) and then sent to the University of California, Irvine, Keck Accelerator Mass Spectrometry Facility for high- precision $\Delta^{14}C$ measurement. One-sigma measurement uncertainty is ~1.8 ‰, equivalent to ~1.2 parts per million (ppm) of recently added fossil fuel–CO_2. $\delta^{13}CO_2$ in PFP samples is measured by dual inlet isotope ratio mass spectrometry with a precision of approximately 0.02 ‰ at the INSTAAR Stable Isotope Laboratory (Vaughn et al., 2004; Sweeney et al., 2015)

Enhancement of each species is defined relative to a time-dependent background level, which is based on nighttime (2 AM local standard time) measurements made at Mount Wilson Observatory (MWO; Fig. 1) located at 1,670 m above sea level. Nighttime air at MWO generally represents the relatively clean, well-mixed free troposphere since polluted LA Basin boundary layer air has typically descended back into the basin by this time. After an additional step of filtering obvious outliers corresponding to pollution events indicated by anomalously elevated values were interpolated to the time of observations within the LA Basin by fitting curves to the screened MWO data (Fig. 2). A further analysis of associated CO measurements indicates that background reconstructed using nighttime air samples from MWO is representative of clean background air coming from either on- or off-shore (Miller et al., 2020).

2.2 Partitioning CO_2 signals using flask-based $\Delta^{14}CO_2$ and $\delta^{13}CO_2$ measurements

Our general approach to distinguishing CO_2 signals from biogenic, petroleum and natural gas sources using $\Delta^{14}CO_2$ and $\delta^{13}CO_2$ follows the procedure described by Newman et al. (2016). Following previous derivations (e.g., Turnbull et al, 2006; Miller et al. 2020), we start with the definition for CO_2ff which is based on mass balances for the atmospherically conserved quantities $\Delta^{14}C\times CO_2$ and CO_2:

$$C_{ff} = \frac{C_{obs}(\Delta_{obs}-\Delta_{bkg})}{(\Delta_{ff}-\Delta_{bkg})} - \frac{C_r(\Delta_r-\Delta_{bkg})}{(\Delta_{ff}-\Delta_{bkg})} \quad (1)$$

Measured CO_2 mole fractions and $\Delta^{14}C$ values are abbreviated as C and Δ. Subscripts 'obs', 'bkg', 'ff' and 'r' represent observations, background, fossil fuel, and respiration, respectively. Δ_{ff} is equal to -1000 ‰. As in the Miller et al. (2020) study focusing on LA, we estimate the value of the small respiratory term, $C_r(\Delta_r - \Delta_{bkg})/(\Delta_{ff} - \Delta_{bkg})$, as 0.25 ppm. The overall uncertainty of C_{ff} for LA measurements during 2015 is approximately 1.2 ppm, which includes 100% uncertainty assigned to the respiratory term. C_{ff} and C_{bio} ($C_{bio} = C_{xs} - C_{ff}$) are calculated for all available flask air samples during the 2014 – 2016 sampling period, a frequency of approximately three times per week at each of the three sites.

C_{ff} is then separated into signals from petroleum and natural gas combustion using ^{13}C:^{12}C ratios ($\delta^{13}C$ as defined by standard isotopic definition; Craig, 1957) measured on the same air samples. First, the flux weighted-mean $\delta^{13}C$ signature of all sources located in the observation footprints (δ_{src}) is determined on a sample-by-sample basis using the combined mass balances for $\delta^{13}C\times CO_2$ and CO_2:

$$\delta_{src} = \frac{\delta_{obs}\times C_{obs} - \delta_{bkg}\times C_{bkg}}{C_{obs} - C_{bkg}} \quad (2)$$

where δ is short-hand for $\delta^{13}CO_2$. The uncertainties in C_{obs}, C_{bkg}, δ_{obs}, and δ_{bkg} are 0.1 ppm, 1.5 ppm, 0.02 ‰, and 0.08 ‰, respectively. The "obs" uncertainties are measurement uncertainties, while the "bkg" uncertainties are determined as the standard deviation of the difference between the observations and their smoothed curve representation at MWO. The median uncertainty in δ_{src} is 3.0 ‰ and is calculated by propagating the uncertainties listed above, including covariance between $\delta^{13}C$ and $\delta^{13}C\times CO_2$.

We combine C_{ff} (eq. 1) and δ_{src} (eq. 2) to determine the $\delta^{13}C$ signature of fossil fuel emissions, δ_{ff}:

$$\delta_{src} = \delta_{ff} \times f_{ff} + \delta_{bio} \times (1 - f_{ff}) \quad (3)$$

Rearranging yields:

$$\delta_{ff} = \frac{\delta_{src} - \delta_{bio} \times (1 - f_{ff})}{f_{ff}} \quad (4)$$

where f is the fraction. Following Newman et al. (2016), we take the isotopic signature of biospheric CO_2 fluxes (δ_{bio}) to be -26.6 ± 0.5 ‰ based on the analysis of Northern Hemisphere mid-latitude CO_2 and $\delta^{13}C$ observations (Bakwin et al., 1998b), which reflects the predominance of C_3 photosynthesis. However, because LA turfgrasses, which could account for a significant fraction of urban CO_2 fluxes [Miller, 2020], are often C_4 species (e.g., Bermuda and Buffalo grasses), we also conduct tests using $\delta_{bio} = -20$ ‰, representing a C3/C4 mix (Fig. S1). When we change δ_{bio} from -26.6 ‰ to -20 ‰, f_{pet} decreases by 0.04 and f_{ng} increases by 0.05 which is smaller than the median uncertainty in f_{pet} and f_{ng} which is 0.17 and 0.16, respectively. f_{ff} is the fraction of C_{ff} in C_{xs}, i.e., C_{ff}/C_{xs}, and $1 - f_{ff} = f_{bio}$. Lastly, the proportion of C_{ff} emitted by petroleum (pet) and natural gas (ng) combustion, f_{pet} and f_{ng}, are calculated from the values of δ_{ff}:

$$\delta_{ff} = \delta_{pet} \times f_{pet/ff} + \delta_{ng} \times (1 - f_{pet/ff}) \quad (5)$$

$$f_{pet/ff} = \frac{\delta_{ff} - \delta_{ng}}{\delta_{pet} - \delta_{ng}} \quad (6)$$

We use values of -25.5 ± 0.5 ‰ for δ_{pet} (Newman et al. 2016; measurements in 2014) and -40.2 ± 0.5 ‰ for δ_{ng} (Newman et al., 2008); $f_{pet} = f_{ff} \times f_{pet/ff}$, and $f_{ng} = f_{ff} \times f_{ng/ff}$, where $f_{ng/ff} = 1 - f_{pet/ff}$. We use temporally constant $\delta^{13}C$ signatures for petroleum, natural gas and biogenic sources (and sinks), although with additional processed-based information, this assumption could be relaxed in the future. Note that although pet, ng, and bio signatures are fixed, both δ_{src} and δ_{ff} vary with time, meaning that f_{bio}, f_{pet} and f_{ng} all vary at the frequency of the air sampling. Samples with calculated $f_{pet/ff}$ values outside the range of 0 and 1, corresponding to small CO_2xs and large uncertainty in δ_{src}, are excluded from the analysis.

2.3 Partitioning CO_2 signals using CO and $\delta^{13}CO_2$ measurements

Although we can determine f_{bio}, f_{pet} and f_{ng} at the frequency of discrete flask sampling events using the method described in Section 2.2, here we describe how comparable CO_2xs fractions can in theory be determined at high frequency using continuous measurements of CO and $\delta^{13}CO_2$. To evaluate the method, we compute the relative contributions of biogenic, petroleum and natural gas sources to CO_2xs using flask air CO and $\delta^{13}CO_2$ measurements and compare these to values obtained using the $\Delta^{14}CO_2$-guided approach for the same samples by applying the following system of equations:

$$R_{src} = R_{bio} \times f_{bio} + R_{pet} \times f_{pet} + R_{ng} \times f_{ng} \quad (7)$$

$$\delta_{src} = \delta_{bio} \times f_{bio} + \delta_{pet} \times f_{pet} + \delta_{ng} \times f_{ng} \quad (8)$$

$$1 = f_{bio} + f_{pet} + f_{ng} \quad (9)$$

R_{src} represents the CO/CO_2 ratio of the total source, which is the observed COxs/CO_2xs ratio, and we use R to refer to the CO/CO_2 emission ratios of individual CO_2xs components (bio, pet, and ng). For now, we assume that R of each source are constant over a year-long period and over the greater LA region (discussed in Section 3.2); especially with high frequency CO and $\delta^{13}CO_2$ measurements, this assumption could easily be relaxed (discussed in Section 3.3).

R values and $\delta^{13}C$ signatures for bio, pet, and ng are needed to solve Eqs. 7-9. $\delta^{13}C$ signatures are specified in section 2.2; R values are obtained via multiple linear regression of Eq. 7 using observed R_{src} and f values determined using $\Delta^{14}C$ and $\delta^{13}C$ of CO_2 measurements as described in Section 2.2. Then we solve Eqs. 7-9 for new f values, f'. This new CO_2xs partitioning (i.e., f'_{bio}, f'_{pet}, f'_{ng}) based on CO and $\delta^{13}CO_2$ observations is used to calculate new values of C_{ff} and C_{bio} (i.e., C'_{ff} and C'_{bio}).

3 Results and Discussion

3.1 Contribution of biogenic, petroleum and natural gas sources in CO_2 excess

We calculated the fractional contribution of petroleum, natural gas, and biospheric fluxes to total CO_2xs each month from April 2015 to March 2016 using $\Delta^{14}CO_2$ and $\delta^{13}CO_2$ observations recorded at FUL, USC and GRA. The results are given in Table S1 and presented in Figure 3. Figure 4 presents the results in terms of the relative CO_2xs contribution from each source at each

site. We observe seasonal variation in CO_2xs from each source. Fossil fuel is the dominant CO_2 emissions source at each site which agrees with the findings of Newman et al. (2016) and Miller et al. (2020). Annually averaged across all three sites, biogenic emissions account for 6 % of CO_2xs. Biogenic emissions are larger and positive in winter and smaller and negative in summer, indicating winter respiration and uptake in summertime, generally consistent with the results of Miller et al. (2020). Note that in this study, we do not partition C_{bio} into an urban biosphere component and other components related to the oxidation of biogenic carbon including ethanol added to gasoline, and human and other animal food and waste (which can only be positive and are unlikely to vary much seasonally). If, as in Miller et al. (2020), we accounted for the always positive ethanol, food, and waste signals, we would likely observe similarly large seasonal drawdown associated with urban vegetation.

We also observe spatial differences: The USC site exhibits a smaller contribution of the biosphere (3 % of annual average CO_2 excess) compared to FUL and GRA (9 % and 5 % of total CO_2 excess, respectively). However, these modest annual average biospheric contributions mask significant seasonal activity. On a monthly basis, maximum positive biogenic contribution is observed in November at 25 %, 26 %, and 22 % at USC, FUL, and GRA (percentage of total CO_2 excess, respectively). And the maximum negative contribution, driven by net photosynthesis, is observed in July with values of -22 %, -13 %, and -12 % at USC, FUL, and GRA (percentage of total CO_2 excess, respectively).

Network average C_{ff} is 11.0 ± 14.5 ppm in winter (November-February; median and standard deviation) and 12.2 ± 6.6 ppm in summer (May-August). No significant difference is observed in winter and summer C_{ff}. This corresponds to the seasonality in Hestia-LA emissions, which indicates C_{ff} inputs are only 3 % higher in winter. High variability observed in wintertime C_{ff} agrees with Miller et al. (2020) which is likely caused by increased temperature inversion trapping as the cold ground surface in winter cools the air layer right above the ground. While Hestia-LA estimated relative contribution of petroleum and natural gas to fossil fuel emissions as 75 % and 25 %, we observe lower contribution of petroleum, 67 %, and larger contribution of natural gas, 33 %. Furthermore, the top-down seasonality of petroleum and natural gas (Fig. 4), which as fractions of C_{ff} should be largely independent of mixing, are clearly evident. The proportion of natural gas in fossil fuel signals are 40 % and 36 % in summer and 34 % and 30% in winter at FUL and USC (Fig. 3). The increase in the natural gas contribution observed in summer can be

explained by the increase in natural gas generated electricity in LA power plants to provide for air conditioning in summer (Newman et al., 2016; He et al., 2019) as well as the air dominantly blowing from southwest during summer. GRA, located northwest of USC by ~35 km without an electricity generation facility nearby, shows the opposite pattern (24 % in summer and 40 % in winter). This suggests the local influence of increased natural gas usage for heating in the winter.

3.2 CO:CO_2 emission ratio (R) values of biogenic, petroleum and natural gas sources

Monthly, site-based R_{src} varies between $5.5 - 11.4$ ppb ppm^{-1} (Fig. 5), with a mean and standard deviation of 8.2 ± 1.6 ppb/ppm (relative s.d. = 19 %). Greater variability is seen in R_{ff} (lower panel): mean and s.d. of 9.6 ± 2.1 ppm (relative s.d. = 22 %). To understand and predict the variation in R_{ff}, we further divide the fossil fuel emissions into petroleum and natural gas emissions. Applying the calculated f values from $\Delta^{14}CO_2$ and $\delta^{13}CO_2$ observations (Section 2.2., Fig. 3), we solve Eq. 7 for each source's CO/CO_2 emission ratio, R (Table 2). Note that we exclude negative flask-based values of COxs (and corresponding R_{src} values) and CO_2ff (and corresponding f_{ff} values) as non-physical. Likewise, positive δ_{src} values and $f_{pet/ff}$ values (and corresponding f_{pet} and f_{ng} values) outside the range of 0-1 are also excluded. A bootstrapping method is used to calculate the mean and uncertainty of possible CO/CO_2 ratios. The CO/CO_2 ratios of petroleum (R_{pet}) and natural gas (R_{ng}) combustion emissions are 12.2 ± 0.6 ppb ppm^{-1} and 2.3 ± 1.2 ppb ppm^{-1}, respectively. As discussed above, the proportion of natural gas in fossil fuel emissions is bigger in summer resulting in smaller R_{ff} in summer at FUL and USC. We find the value of 1.8 ± 0.8 ppb ppm^{-1} for R_{bio} which is non-zero because biofuel (mainly corn-based ethanol) in the gasoline in California with large CO/CO_2 ratio signal is included in the biogenic sources while respiratory CO/CO_2 ratios approach 0. A larger contribution of the biosphere with a low CO/CO_2 ratio in winter offsets the large R_{ff} lowering the variability in R_{src} at each site.

We compare our model-determined CO/CO_2 ratios of each source (Table 2) to bottom-up inventory-based estimates (Table 1). CO/CO_2 ratios of each source constrained from our model and observational data approach agree well with the bottom-up inventory-based estimates. Sources contributing a high percentage of CO_2 emissions strongly influence the total CO/CO_2 ratio. The CO/CO_2 ratio of petroleum combustion is greatly affected by on-road emissions and industrial emissions (contributing 60 % and 28 % of total petroleum CO_2 emissions). Natural gas is mostly

dominated by non-mobile emissions (Electricity production, residential, commercial, and industrial, sequentially) resulting in low CO/CO_2 ratio.

3.3 Estimation of CO_2ff based on CO and $^{13}CO_2$ observations

Table 2 shows the CO/CO_2 ratio and $\delta^{13}C$ signature of each source. The combination of the R and δ signals reveal a distinct pattern for each source: the biosphere has low near-zero R, petroleum has high R, and natural gas has low R. Petroleum and biosphere CO_2 have similar δ values, whereas natural gas has a very low δ. By substituting these values into Eqs. 7-9, f' values are calculated, and then we calculate C'_{ff} by multiplying the sum of f'_{pet} and f'_{ng} by CO_2xs measured every few days. We compare f'_{ff} and C'_{ff} to f_{ff} and C_{ff} (determined using ^{14}C observations) in Fig. 6. Assessment for each source is shown in Figure S2 and S3. The R^2 values are 0.63 and 0.90 for f'_{ff} and C'_{ff}, respectively.

If R values are allowed to vary in time, it is likely to improve the precision of the method. We calculate the uncertainty in C'_{ff} for varying temporal resolutions of R (black solid line in Fig. 7). We find that the uncertainty increases when the size of the window increases from 1-week to 10-week; in other words, allowing temporal variation in R improves the precision of the method. However, the uncertainty slightly decreases beyond the 10-week window. This is likely caused by the reduction in the error of R values (not shown) as the number of observations used to find R (by solving Eq. 7) increases. In summary, the ideal flask sampling frequency for this method would be higher than every 2 weeks. In cases where this is impossible, it is better to assume constant R values.

The uncertainty in C'_{ff} estimated using the CO-based method is also shown in Figure 7 (black dashed line). The CO-based method also provides improved precision of the method when flask sampling is available at higher frequency. However, the CO and $\delta^{13}CO_2$-based method shows greater confidence than the CO-based method for the whole range of adjusted temporal resolution in R. When using constant R values (temporal resolution of 50 weeks), the uncertainty is 3.2 ppm (the 1σ standard deviation of differences between C_{ff} and C'_{ff}) for the CO and $\delta^{13}CO_2$-based method, while it is 4.8 ppm for CO-based method. This improvement is likely associated with the additional information provided by $\delta^{13}CO_2$ that constrains the effective R_{ff} and further separates fossil fuel sources into sub-categories (petroleum and natural gas sources).

4 Conclusions

We present a CO and $\delta^{13}CO_2$-based method to estimate CO_2ff which is based on flask-based $\Delta^{14}CO_2$ measurements. We have applied the method to measurements from flask samples collected in the LA basin, every few days in the afternoon for more than one year (2015-16). The proposed method was assessed by comparing it to a more traditional $\Delta^{14}CO_2$-based method. CO and $\delta^{13}CO_2$ approach can be applied to continuous measurements of CO_2, CO and $\delta^{13}CO_2$ which can provide CO_2ff estimates at higher temporal resolution and with greater accuracy than previously applied CO-based methods.

We have analyzed three locations in the Los Angeles megacity, partitioning observed CO_2 enhancements (CO_2xs) into biogenic, petroleum and natural gas sources. We observed a substantial biogenic signal that varies from -14% to +25% of CO_2xs over the course of the year, with positive contributions in winter and negative contributions in summer due to net respiration and net photosynthesis, respectively. Furthermore, partitioning CO_2ff into petroleum and natural gas combustion fractions revealed that natural gas combustion has the largest contribution in summer, potentially due to an increase in electricity generation at LA power plants for air conditioning.

Data availability. The data that support the findings of this study are available from JBM (john.b.miller@noaa.gov) upon request.

Author contributions. JK designed and executed the study. JBM, SJL, and SEM provided the data. JK prepared the manuscript with contributions from all co-authors

Competing interests. The authors declare that they have no conflict of interest.

References

Ahn, D. Y., Hansford, J. R., Howe, S. T., Ren, X. R., Salawitch, R. J., Zeng, N., Cohen, M. D., Stunder, B., Salmon, O. E., Shepson, P. B., Gurney, K. R., Oda, T., Lopez-Coto, I., Whetstone, J., and Dickerson, R. R.: Fluxes of Atmospheric Greenhouse-Gases in Maryland (FLAGG-MD): Emissions of Carbon Dioxide in the Baltimore, MD-Washington, D.C. Area, J. Geophys. Res.

Atmos., 125, 1–23, https://doi.org/10.1029/2019JD032004, 2020.

Bakwin, P. S., Tans, P. P., Andres, J., and Conway, C. O.: Determination of the isotopic (13C/12C) discrimination of atmospheric, Global Biogeochem. Cycles, 12, 555–562, 1998a.

Bakwin, P. S., Tans, P. P., White, J. W. C., and Andres, R. J.: Determination of the isotopic (13C/12C) discrimination of terrestrial biology from a global network of observations, Global Biogeochem. Cycles, 12, https://doi.org/10.1029/98GB02265, 1998b.

Bréon, F. M., Broquet, G., Puygrenier, V., Chevallier, F., Ramonet, M., Dieudonné, E., Lopez, M., Cea-cnrs-uvsq, U. M. R., and Yvette, G.: An attempt at estimating Paris area CO2 emissions from atmospheric concentration measurements, Atmos. Chem. Phys., 1707–1724, https://doi.org/10.5194/acp-15-1707-2015, 2015.

Cambaliza, M. O. L., Shepson, P. B., Caulton, D. R., Stirm, B., Samarov, D., Gurney, K. R., Turnbull, J. C., Davis, K. J., Possolo, A., Karion, A., Sweeney, C., Moser, B., Hendricks, A., Lauvaux, T., Mays, K., Whetstone, J., Huang, J., Razlivanov, I., Miles, N. L., and Richardson, S. J.: Assessment of uncertainties of an aircraft-based mass balance approach for quantifying urban greenhouse gas emissions, Atmos. Chem. Phys., 14, 9029–9050, https://doi.org/10.5194/acp-14-9029-2014, 2014.

Craig, H.: Isotopic standards for carbon and oxygen and correction factors for mass-spectrometric analysis of carbon dioxide, Geochim. Cosmochim. Acta, 12, https://doi.org/10.1016/0016-7037(57)90024-8, 1957.

Djuricin, S., Pataki, D. E., and Xu, X.: A comparison of tracer methods for quantifying CO2 sources in an urban region, J. Geophys. Res., 115, 1–13, https://doi.org/10.1029/2009JD012236, 2010.

Fleisher, A. J., Long, D. A., Liu, Q., Gameson, L., and Hodges, J. T.: Optical Measurement of Radiocarbon below Unity Fraction Modern by Linear Absorption Spectroscopy, J. Phys. Chem. Lett., 8, https://doi.org/10.1021/acs.jpclett.7b02105, 2017.

Gately, C. K. and Hutyra, L. R.: Large Uncertainties in Urban-Scale Carbon Emissions, J. Geophys. Res. Atmos., 122, 11,242-11,260, https://doi.org/10.1002/2017JD027359, 2017.

Genoud, G., Lehmuskoski, J., Bell, S., Palonen, V., Oinonen, M., Koskinen-Soivi, M. L., and Reinikainen, M.: Laser Spectroscopy for Monitoring of Radiocarbon in Atmospheric Samples, Anal. Chem., 91, https://doi.org/10.1021/acs.analchem.9b02496, 2019.

Gourdji, S. M., Karion, A., Lopez-Coto, I., Ghosh, S., Mueller, K. L., Zhou, Y., Williams, C. A.,

Baker, I. T., Haynes, K. D., and Whetstone, J. R.: A Modified Vegetation Photosynthesis and Respiration Model (VPRM) for the Eastern USA and Canada, Evaluated With Comparison to Atmospheric Observations and Other Biospheric Models, J. Geophys. Res. Biogeosciences, 127, https://doi.org/10.1029/2021JG006290, 2022.

Graven, H. D., Stephens, B. B., Guilderson, T. P., Campos, T. L., Schimel, D. S., Campbell, J. E., and Keeling, R. F.: Vertical profiles of biospheric and fossil fuel-derived CO2 and fossil fuel CO2: CO ratios from airborne measurements of Δ14C, CO2 and CO above Colorado, USA, Tellus, Ser. B Chem. Phys. Meteorol., 61, https://doi.org/10.1111/j.1600-0889.2009.00421.x, 2009.

Gurney, K. R., Patarasuk, R., Liang, J., Song, Y., O'Keeffe, D., Rao, P., Whetstone, J. R., Duren, R. M., Eldering, A., and Miller, C. E.: The Hestia Fossil Fuel CO2 Emissions Data Product for the Los Angeles Megacity (Hestia-LA), Earth Syst. Sci. Data, 11, 1309–1335, https://doi.org/10.5194/essd-2018-162, 2019.

Hardiman, B. S., Wang, J. A., Hutyra, L. R., Gately, C. K., Getson, J. M., and Friedl, M. A.: Accounting for urban biogenic fluxes in regional carbon budgets, Sci. Total Environ., 592, 366–372, https://doi.org/10.1016/j.scitotenv.2017.03.028, 2017.

He, L., Zeng, Z., Pongetti, T. J., Wong, C., Liang, J., Gurney, K. R., Newman, S., Yadav, V., Verhulst, K. R., Miller, C. E., Duren, R., Frankenberg, C., Wennberg, P. O., Shia, R., Yung, Y. L., and Sander, S. P.: Atmospheric Methane Emissions Correlate With Natural Gas Consumption From Residential and Commercial Sectors in Los Angeles, Geophys. Res. Lett., 46, 8563–8571, https://doi.org/10.1029/2019gl083400, 2019.

Heimburger, A., Harvey, R., Shepson, P. B., Stirm, B. H., Gore, C., Turnbull, J. C., Cambaliza, M. O. L., Salmon, O. E., Kerlo, A.-E. M., Lavoie, T. N., Davis, K. J., Lauvaux, T., Karion, A., Sweeney, C., Brewer, W. A., Hardesty, R. M., and Gurney, K. R.: Assessing the optimized precision of the aircraft mass balance method for measurement of urban greenhouse gas emission rates through averaging, Elem Sci Anth, 5, 26, https://doi.org/10.1525/elementa.134, 2017.

Lauvaux, T., Miles, N. L., Deng, A., Richardson, S. J., Cambaliza, M. O., Davis, K. J., Gaudet, B., Gurney, K. R., Huang, J., O'Keefe, D., Song, Y., Karion, A., Oda, T., Patarasuk, R., Razlivanov, I., Sarmiento, D., Shepson, P., Sweeney, C., Turnbull, J. C., and Wu, K.: High-resolution atmospheric inversion of urban CO2 emissions during the dormant season of the Indianapolis flux experiment (INFLUX), J. Geophys. Res., 121, 5213–5236,

https://doi.org/10.1002/2015JD024473, 2016.

Lauvaux, T., Gurney, K. R., Miles, N. L., Davis, K. J., Richardson, S. J., Deng, A., Nathan, B. J., Oda, T., Wang, J. A., Hutyra, L., and Turnbull, J. C.: Policy-relevant assessment of urban CO2emissions, Environ. Sci. Technol., 54, 10237–10245, https://doi.org/10.1021/acs.est.0c00343, 2020.

Lehman, S. J., Miller, J. B., Wolak, C., Southon, J., Tans, P. P., Montzka, S. A., Sweeney, C., Andrews, A., LaFranchi, B., Guilderson, T. P., and Turnbull, J. C.: Allocation of Terrestrial Carbon Sources Using 14 CO 2 : Methods, Measurement, and Modeling, Radiocarbon, 55, https://doi.org/10.1017/s0033822200048414, 2013.

Levin, I. and Karstens, U.: Inferring high-resolution fossil fuel CO2 records at continental sites from combined 14CO2 and CO observations, Tellus, Ser. B Chem. Phys. Meteorol., 59, 245–250, https://doi.org/10.1111/j.1600-0889.2006.00244.x, 2007.

Lopez, M., Schmidt, M., Delmotte, M., Colomb, A., Gros, V., Janssen, C., Lehman, S. J., Mondelain, D., Perrussel, O., Ramonet, M., Xueref-Remy, I., and Bousquet, P.: CO, NOx and 13CO2 as tracers for fossil fuel CO2: Results from a pilot study in Paris during winter 2010, Atmos. Chem. Phys., 13, 7343–7358, https://doi.org/10.5194/acp-13-7343-2013, 2013.

Mays, K. L., Shepson, P. B., Stirm, B. H., Karion, A., Sweeney, C., and Gurney, K. R.: Aircraft-based measurements of the carbon footprint of Indianapolis, Environ. Sci. Technol., 43, 7816–7823, https://doi.org/10.1021/es901326b, 2009.

McCartt, A. D. and Jiang, J.: Room-Temperature Optical Detection of 14CO2below the Natural Abundance with Two-Color Cavity Ring-Down Spectroscopy, ACS Sensors, 7, https://doi.org/10.1021/acssensors.2c01253, 2022.

Mcdonald, B. C., McBride, Z. C., Martin, E. W., and Harley, R. A.: High-resolution mapping of motor vehicle carbon dioxide emissions, J. Geophys. Res. Atmos., 5283–5298, https://doi.org/10.1002/2013JD021219.Received, 2014.

Miller, J. B., Lehman, S. J., Montzka, S. A., Sweeney, C., Miller, B. R., Karion, A., Wolak, C., Dlugokencky, E. J., Southon, J., Turnbull, J. C., and Tans, P. P.: Linking emissions of fossil fuel CO2 and other anthropogenic trace gases using atmospheric 14CO2, J. Geophys. Res. Atmos., 117, https://doi.org/10.1029/2011JD017048, 2012.

Miller, J. B., Lehman, S. J., Verhulst, K. R., Miller, C. E., Duren, R. M., Yadav, V., Newman, S., and Sloop, C. D.: Large and seasonally varying biospheric CO2 fluxes in the Los Angeles

megacity revealed by atmospheric radiocarbon, Proc. Natl. Acad. Sci. U. S. A., 117, 26681–26687, https://doi.org/10.1073/pnas.2005253117, 2020.

Newman, S. and Jeong, S.: Diurnal tracking of anthropogenic CO2 emissions in the Los Angeles basin megacity during spring 2010, Atmos. Chem. Phys., 4359–4372, https://doi.org/10.5194/acp-13-4359-2013, 2013.

Newman, S., Xu, X., Affek, H. P., Stolper, E., and Epstein, S.: Changes in mixing ratio and isotopic composition of CO2 in urban air from the Los Angeles basin, California, between 1972 and 2003, J. Geophys. Res. Atmos., 113, 1–15, https://doi.org/10.1029/2008JD009999, 2008.

Newman, S., Xu, X., Gurney, K. R., Hsu, Y. K., Li, K. F., Jiang, X., Keeling, R. F., Feng, S., O'Keefe, D., Patarasuk, R., Wong, K. W., Rao, P., Fischer, M. L., and Yung, Y. L.: Toward consistency between trends in bottom-up CO2 emissions and top-down atmospheric measurements in the Los Angeles megacity, Atmos. Chem. Phys., 16, 3843–3863, https://doi.org/10.5194/acp-16-3843-2016, 2016.

Sargent, M., Barrera, Y., Nehrkorn, T., Hutyra, L. R., Gately, C. K., Jones, T., McKain, K., Sweeney, C., Hegarty, J., Hardiman, B., and Wofsy, S. C.: Anthropogenic and biogenic CO2 fluxes in the Boston urban region, Proc. Natl. Acad. Sci., 115, 7491–7496, https://doi.org/10.1073/pnas.1803715115, 2018.

Staufer, J., Broquet, G., Bréon, F. M., Puygrenier, V., Chevallier, F., Xueref-remy, I., Dieudonné, E., Lopez, M., Schmidt, M., Ramonet, M., Perrussel, O., Lac, C., Wu, L., and Ciais, P.: The first 1-year-long estimate of the Paris region fossil fuel CO2 emissions based on atmospheric inversion, Atmos. Chem. Phys., 14703–14726, https://doi.org/10.5194/acp-16-14703-2016, 2016.

Stuiver, M. and Polach, H. A.: Discussion: Reporting of 14C Data, Radiocarbon, 19, 355–363, 1977.

Super, I., Dellaert, S. N. C., Visschedijk, A. J. H., and Van Der Gon, H. A. C. D.: Uncertainty analysis of a European high-resolution emission inventory of CO2 and CO to support inverse modelling and network design, Atmos. Chem. Phys., 20, https://doi.org/10.5194/acp-20-1795-2020, 2020.

Sweeney, C., Karion, A., Wolter, S., Newberger, T., Guenther, D., Higgs, J. A., Andrews, A. E., Lang, P. M., Neff, D., Dlugokencky, E., Miller, J. B., Montzka, S. A., Miller, B. R., Masarie, K. A., Biraud, S. C., Novelli, P. C., Crotwell, M., Crotwell, A. M., Thoning, K., and Tans, P. P.:

Seasonal climatology of CO2 across North America from aircraft measurements in the NOAA/ESRL Global Greenhouse Gas Reference Network, J. Geophys. Res. Atmos., 5155–5190, https://doi.org/10.1002/2014JD022591.Received, 2015.

Turnbull, J. C., Karion, A., Fischer, M. L., Faloona, I., Guilderson, T., Lehman, S. J., and Miller, B. R.: Assessment of fossil fuel carbon dioxide and other anthropogenic trace gas emissions from airborne measurements over Sacramento, California in spring 2009, Atmos. Chem. Phys., 705–721, https://doi.org/10.5194/acp-11-705-2011, 2011.

Turnbull, J. C., Sweeney, C., Karion, A., Newberger, T., Lehman, S. J., Tans, P. P., Davis, K. J., Lauvaux, T., Miles, N. L., Richardson, S. J., Cambaliza, M. O., Shepson, P. B., Gurney, K. R., Patarasuk, R., and Razlivanov, I.: Toward quantification and source sector identification of fossil fuel CO2 emissions from an urban area: Results from the INFLUX experiment, J. Geophys. Res., 120, 292–312, https://doi.org/10.1002/2014JD022555, 2015.

Turnbull, J. C., Karion, A., Davis, K. J., Lauvaux, T., Miles, N. L., Richardson, S. J., Sweeney, C., McKain, K., Lehman, S. J., Gurney, K. R., Patarasuk, R., Liang, J., Shepson, P. B., Heimburger, A., Harvey, R., and Whetstone, J.: Synthesis of Urban CO2 Emission Estimates from Multiple Methods from the Indianapolis Flux Project (INFLUX), Environ. Sci. Technol., 53, 287–295, https://doi.org/10.1021/acs.est.8b05552, 2019.

Turnbull, J. C., DeCola, P., Mueller, K., and Vogel, F.: IG3IS Urban Greenhouse Gas Emission Observation and Monitoring Best Research Practices, World Meteorological Organization, 2022.

Turner, A. J., Kim, J., Fitzmaurice, H., Newman, C., Worthington, K., Chan, K., Wooldridge, P., Köhler, P., Frankenberg, C., and Cohen, R. C.: Observed impacts of COVID-19 on urban CO2 emissions, Geophys. Res. Lett., 2–10, 2020.

Vardag, S. N., Gerbig, C., Janssens-Maenhout, G., and Levin, I.: Estimation of continuous anthropogenic CO2: Model-based evaluation of CO2, CO, δ13C(CO2) and Δ14C(CO2) tracer methods, Atmos. Chem. Phys., 15, 12705–12729, https://doi.org/10.5194/acp-15-12705-2015, 2015.

Vaughn, B. H., Miller, J. B., Ferretti, D. F., and White, J. W. C.: Stable isotope measurements of atmospheric CO2 and CH4, in: Handbook of Stable Isotope Analytical Techniques, https://doi.org/10.1016/B978-044451114-0/50016-8, 2004.

Vimont, I. J., Turnbull, J. C., Petrenko, V. V., Place, P. F., Sweeney, C., Miles, N., Richardson, S., Vaughn, B. H., and White, J. W. C.: An improved estimate for the δc and δc signatures of

carbon monoxide produced from atmospheric oxidation of volatile organic compounds, Atmos. Chem. Phys., 19, 8547–8562, https://doi.org/10.5194/acp-19-8547-2019, 2019.

Vogel, F. R., Hammer, S., Steinhof, A., Kromer, B., and Levin, I.: Implication of weekly and diurnal 14C calibration on hourly estimates of CO-based fossil fuel CO2 at a moderately polluted site in southwestern Germany, Tellus, Ser. B Chem. Phys. Meteorol., 62, 512–520, https://doi.org/10.1111/j.1600-0889.2010.00477.x, 2010.

Vogel, F. R., Frey, M., Staufer, J., Hase, F., Broquet, G., and Xueref-remy, I.: XCO2 in an emission hot-spot region : the COCCON Paris campaign 2015, Atmos. Chem. Phys., 19, 3271–3285, 2019.

Winbourne, J. B., Smith, I. A., Stoynova, H., Kohler, C., Gately, C. K., Logan, B. A., Reblin, J., Reinmann, A., Allen, D. W., and Hutyra, L. R.: Quantification of Urban Forest and Grassland Carbon Fluxes Using Field Measurements and a Satellite-Based Model in Washington DC/Baltimore Area, J. Geophys. Res. Biogeosciences, 127, https://doi.org/10.1029/2021JG006568, 2022.

Wu, D., Lin, J. C., Duarte, H. F., Yadav, V., Parazoo, N. C., Oda, T., and Kort, E. A.: A model for urban biogenic CO2 fluxes: Solar-Induced Fluorescence for Modeling Urban biogenic Fluxes (SMUrF v1), Geosci. Model Dev., 14, https://doi.org/10.5194/gmd-14-3633-2021, 2021.

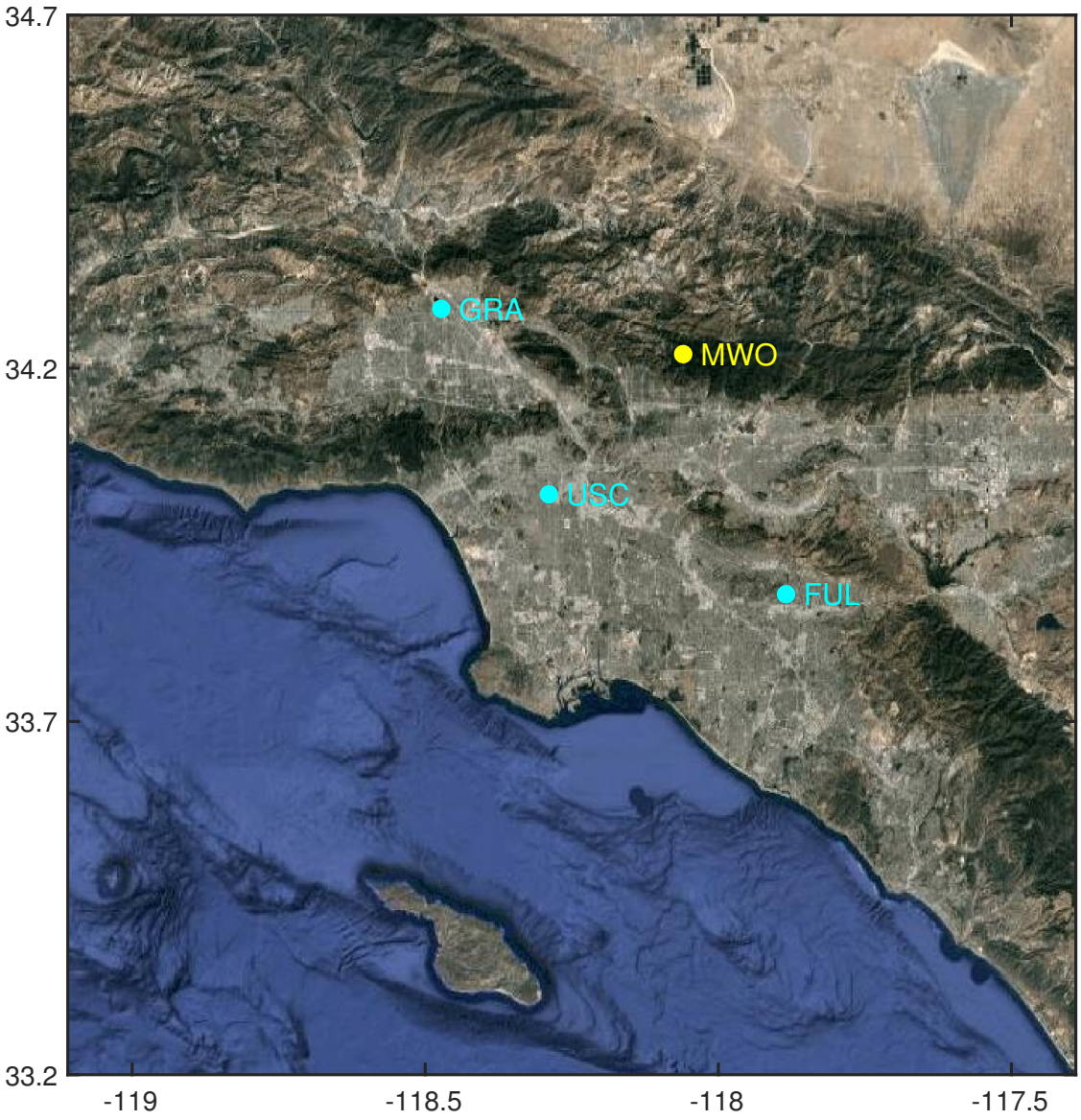

Figure 1. Map of the greater Los Angeles region. The three Los Angeles Megacity Carbon Project sites are marked in cyan and the Mount Wilson Observatory used to define background values are marked in yellow. Map data © Google Maps 2022.

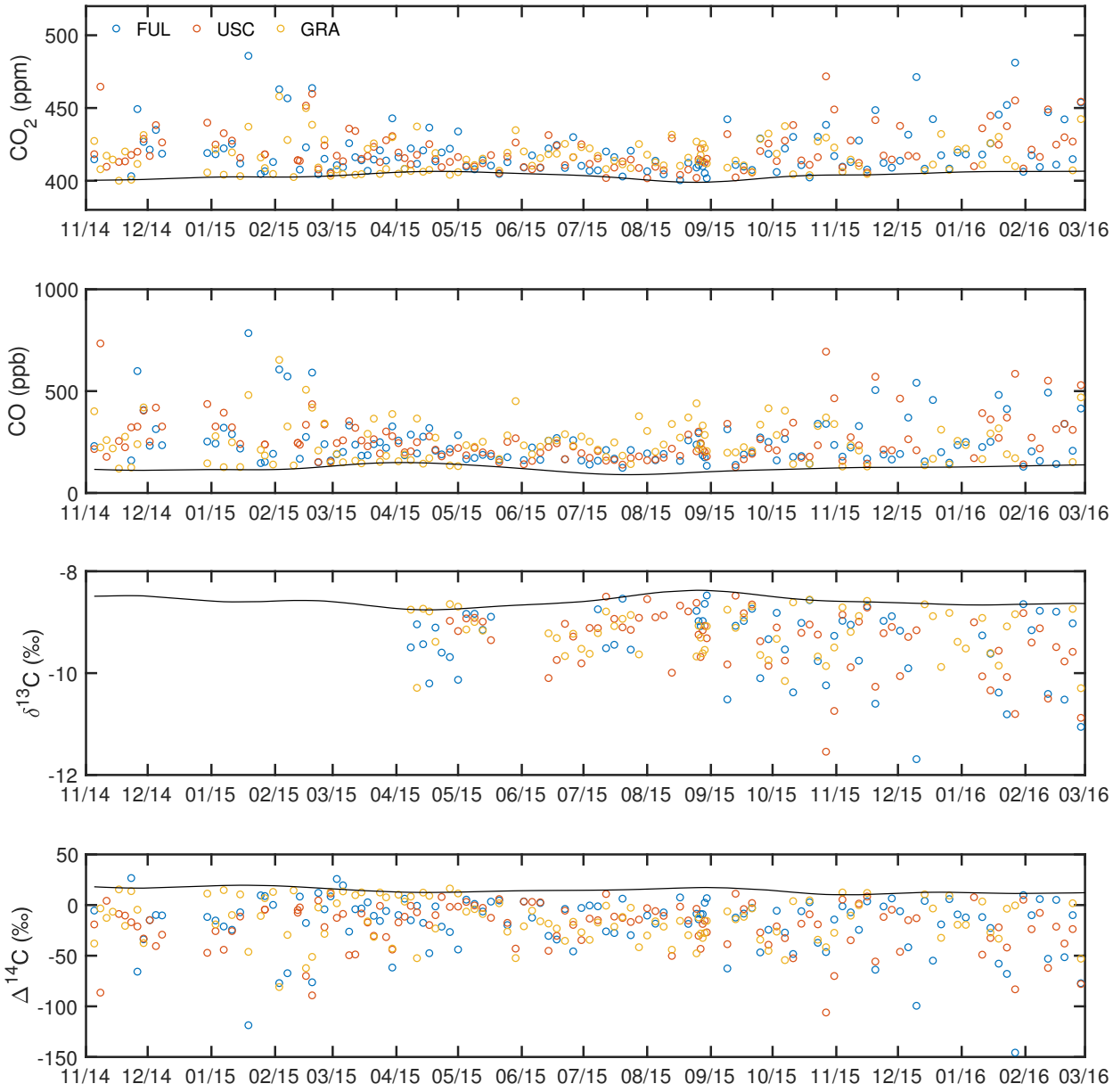

Figure 2. Timeseries of CO_2, CO, $\delta^{13}C$, and $\Delta^{14}C$. Black line represents background values. Dates are labeled in month/year.

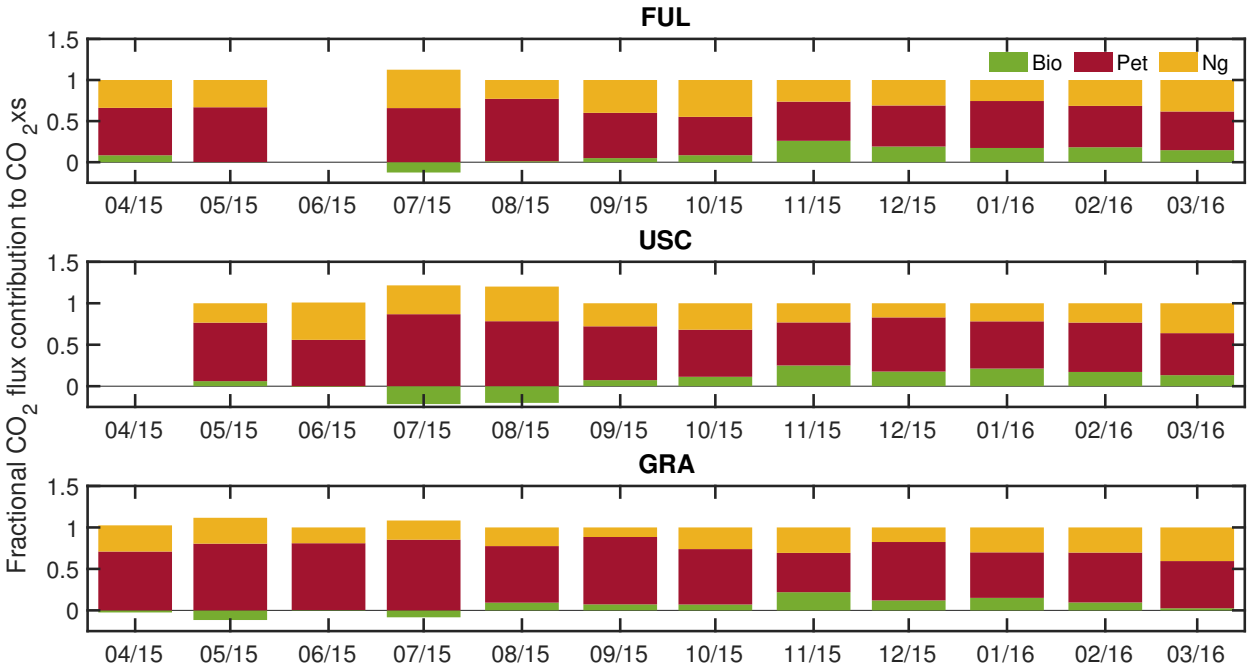

Figure 3. Monthly mean fractional contributions (f) of biosphere (green), petroleum (red), and natural gas (yellow) to CO_2xs at each site, as determined from $\Delta^{14}C$ and $\delta^{13}C$ observations (Section 2.2). The sum of the fractions is one in each month. Dates are labeled in month/year.

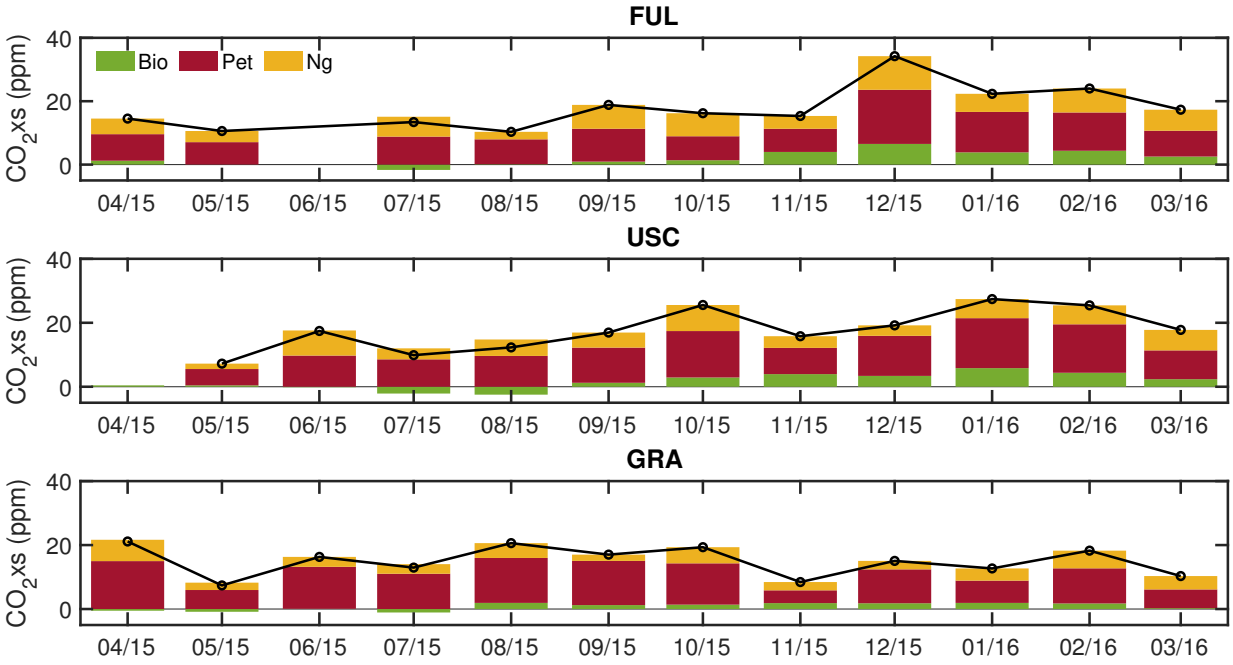

Figure 4. Monthly mean CO_2xs partitioned into biosphere (green), petroleum (red), and natural gas (yellow) signals, as determined from $\Delta^{14}C$ and $\delta^{13}C$ observations, at each site. The black marker indicates CO_2xs. Dates are labeled in month/year.

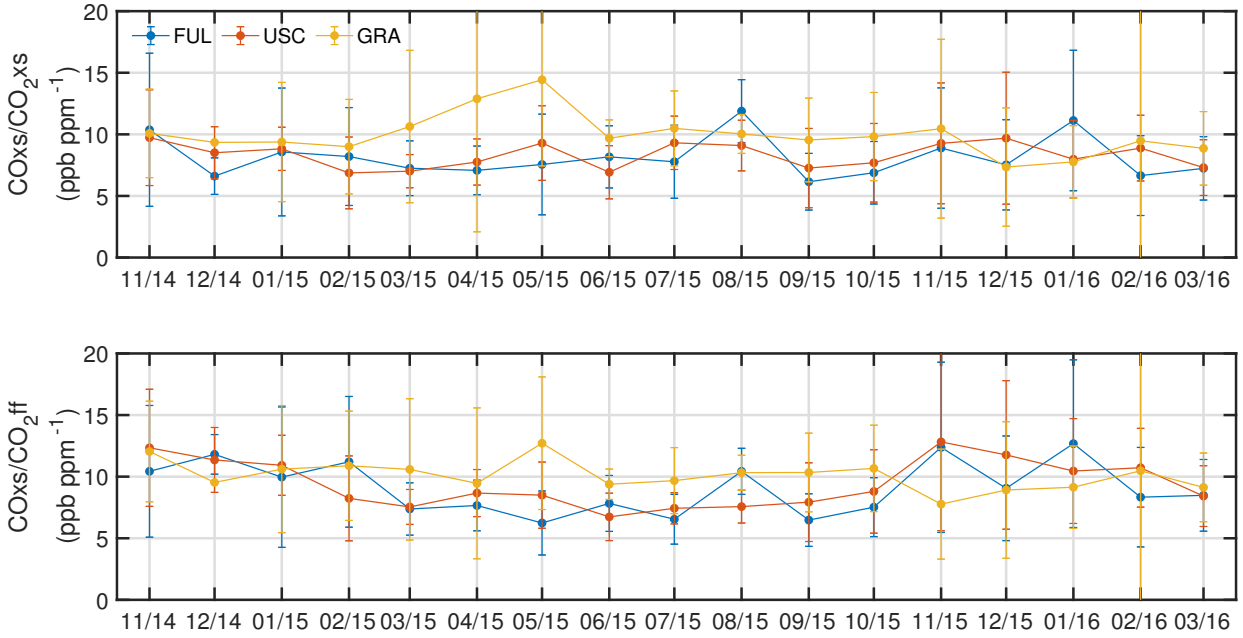

Figure 5. Monthly variations in $COxs/CO_2xs$ (Rsrc) and $COxs/CO_2ff$ (Rff) at each site. $COxs/CO_2ff$ is calculated using ^{14}C observations. Dates are labeled in month/year.

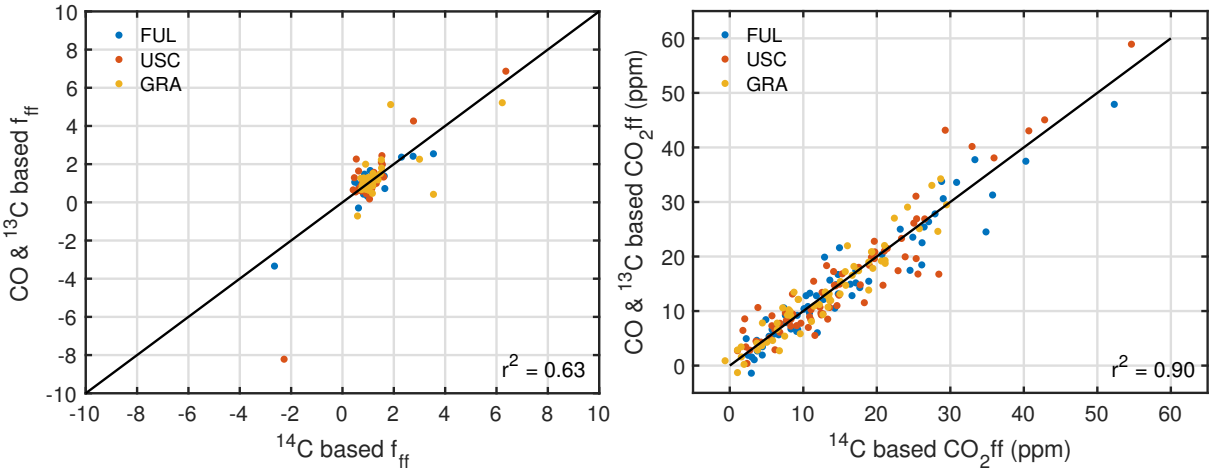

565

Figure 6. Comparison of f_{ff} and f'_{ff} (left) and C_{ff} and C'_{ff} (right). Black lines represent 1:1 relationships and different colors indicate different sites.

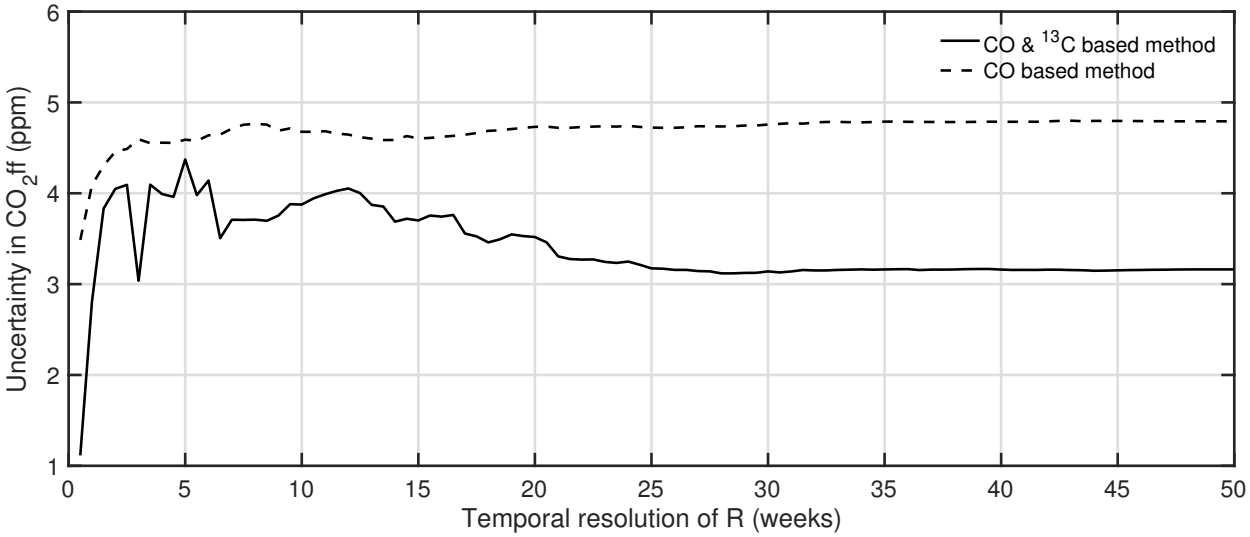

570

Figure 7. Uncertainty in C'_{ff} for varying temporal resolution of R (N weeks). R is determined for each data point solving Eq. 7 using CO, $^{13}CO_2$ and $^{14}CO_2$ observations within a moving window of 2N weeks. For CO-based method, R_{ff} is smoothed using a 2N weeks moving window.

575

Table 1. Bottom-up CO_2 emission, CO emission, and R (CO/CO_2 ratio) estimates for each source sector and fuel type for LA basin based on the Vulcan 3.0 and the U.S. Environmental Protection Agency (EPA) National Emission Inventory for 2011 (NEI 2011) product. NEI 2011 is scaled by the emissions with fuel consumption dataset from the U.S. Energy Information Administration (EIA) State Energy Data System (SEDS) to estimate 2015 CO emissions.

	----------Petroleum----------			----------Natural Gas----------		
	CO_2 (MtC)	CO (MtC)	R = CO/CO_2 (ppb ppm^{-1})	CO_2 (MtC)	CO (MtC)	R = CO/CO_2 (ppb ppm^{-1})
Residential	0.06	<0.001	0.03	2.79	0.001	0.52
Commercial	0.67	<0.001	0.15	1.79	0.002	1.09
Industrial	9.79	<0.001	0.02	1.59	0.002	1.28
Electricity Production	0.37	<0.001	0.02	5.08	0.002	0.32
On-road	20.97	0.296	13.62	0	0	
Non-road	1.45	0.139	96.05	0.19	0.012	65.32
Airport	0.89	0.008	9.27	0	0	
Rail	0.47	0.002	5.12	0	0	
CMV	0.48	<0.001	1.40	0	0	
Total	**35.16**	**0.437**	**12.42**	**11.44**	**0.019**	**1.68**

585 **Table 2.** CO/CO_2 ratios (R) and $\delta^{13}C$ signatures used to determine relative contribution of biogenic, petroleum and natural gas sources.

	Biosphere	Petroleum	Natural Gas
Bottom-up approach R (ppb ppm^{-1})[a]		12.4	1.7
Top-down approach R (ppb ppm^{-1})[b]	1.8 ± 0.8	12.2 ± 0.6	2.3 ± 1.2
$\delta^{13}C$ (‰)[c]	-26.6 ± 0.5	-25.5 ± 0.5	-40.2 ± 0.5

[a]R calculated from Table 1. These values are not used for CO_2xs partitioning and are for
590 reference only.
[b]R calculated from CO, $\delta^{13}CO_2$ and $\Delta^{14}CO_2$ flask observations. These values are used in this study.
[c]$\delta^{13}C$ from previous studies (Bakwin et al., 1998a; Newman et al., 2008)